New LYNRED Engine solution for Optical Gas Imaging: ATI EOLE

Adrien Bertrand, Gabriel Jobert, Charlène Lefèvre, Nicolas Vannier, Benoit Louvat, Eric Mallet

New LYNRED Engine solution for Optical Gas Imaging: ATI EOLE

Adrien Bertrand*[a], Gabriel Jobert[a], Charlène Lefèvre[a], Nicolas Vannier[a], Benoit Louvat[a], Eric Mallet[a]
[a]LYNRED, 364 Avenue de Valence, Actipole CS 10021, 38113 Veurey-Voroize; France
*Adrien.bertrand@LYNRED.com; Phone +33 6 62 14 68 14; LYNRED.com

ABSTRACT

As international regulations on methane emissions evolve, LYNRED introduces EOLE: a state-of-the-art VGA (640x512/15µm) HOT-MWIR sensor dedicated to hydrocarbon optical gas imaging (OGI). This paper aims to provide valuable insights into the technical advancements and practical applications of our technologies in the ongoing effort to monitor and mitigate methane emissions.

We introduce the theoretical principles of OGI and key performance metrics, such as noise equivalent concentration-length (NECL) and minimal detectable leak-rate (MDLR). Performance simulations show a state-of-the-art NECL and MDLR<1g/h, compliant with Type 2 leak detection and repair (LDAR) for EOLE.

ATI (Advanced Thermal Imager) EOLE is a module that features embedded video pipeline, including image correction, denoising, and colorization. Such advanced algorithms provide the user with a clear image of the plume, with enhanced sensitivity, to locate or quantify a gas leak. LYNRED Toolbox software includes further visual enhancement tools capable to display the faintest leaks in complex situations. In this paper, we demonstrate the sensor sensitivity and algorithms capabilities on real, controlled, methane plumes of different leak rates.

Additionally, we present our innovative solution to the need for SWaP (Size, Weight, and Power). The launch of the PlugUp™ platform in late 2024 demonstrates LYNRED's commitment to provide compact and versatile imaging cores.

By addressing regulatory requirements and market needs, LYNRED's solutions position themselves as critical tools for effective methane surveillance, contributing to environmental protection and compliance with emerging standards.

Keywords: LYNRED, ATI EOLE, PlugUp, OGI, Algorithms, Infrared, Engine

1. INTRODUCTION

Methane (CH_4) is a potent greenhouse gas with a global warming potential significantly higher than carbon dioxide (CO_2). Reducing methane emissions is a critical component of climate change mitigation strategies, particularly in the energy sector, where fugitive emissions from oil and gas operations represent a major source of anthropogenic methane emission. Recognizing this urgency, regulatory bodies in both the United States and the European Union have implemented new policies aimed at improving methane detection and mitigation.

In the United States, the Environmental Protection Agency (EPA) has introduced stringent regulations under the New Source Performance Standards (NSPS) Quad Os, which expand leak detection and repair (LDAR) requirements, and incorporate the use of advanced methane detection technologies.

This regulation calls for specific performance criteria for Optical Gas Imaging (OGI) cameras. The technical requirements for these cameras are detailed in Appendix K of the Final Rule (2022) [1], which prescribes the conditions under which methane emissions must be identifiable using OGI technology. According to the EPA standard, an OGI camera must be capable of detecting or producing a detectable image of methane emissions at a minimum threshold of 19 g/h. Furthermore, the regulation specifies alternative hydrocarbon detection thresholds to account for different chemical compositions of fugitive emissions. In particular, the camera must be able to detect n-butane emissions of 29 g/h or propane emissions of 22 g/h. These detection thresholds must be met under controlled environmental conditions, including:

- Viewing distance: 2.0 meters
- Gas-to-background temperature differential (ΔT): 5.0 °C
- Wind conditions: ≤ 1.0 m/s (calm wind conditions)

The need to give a specific temperature differential and wind conditions highlights the influence of environmental factors on the detection capabilities of thermal imaging technologies.

Concurrently, the European Union has enacted Regulation (EU) 2024/1787, a legislative framework designed to enforce comprehensive LDAR programs, prohibit routine venting and flaring, and mandate greater transparency in methane emissions along fossil fuel supply chains. This regulation aligns with the EU's broader climate policy objectives, ensuring accountability for both domestic and imported fossil energy sources.

Unlike the EPA's singular threshold for OGI camera performance, the EU regulation classifies LDAR requirements into two distinct categories, each with different methane leak detection thresholds:

- Type 1 LDAR: Minimal detectable leak rate of 17 g/h
- Type 2 LDAR: Minimal detectable leak rate of 1 g/h

These classifications distinguish between general-purpose leak detection (Type 1) and highly sensitive monitoring (Type 2), which may be required for high-risk infrastructure or critical emission sources. Notably, Regulation EU/2024/1787 does not explicitly specify a gas-to-background temperature differential (ΔT) for methane detection.

Considering the evolution of LDAR regulations, LYNRED has been focusing on offering a sensitive OGI solution that answers to the above-mentioned requirements. In June 2024, LYNRED has therefore launched its EOLE product, a cooled VGA (640x512) 15µm pixel pitch sensitive in the 3.2 to 3.55µm spectral band. Indeed, methane exhibits a strong absorption band in the MWIR range, around 3.3µm, as shown in Figure 1. This absorption band is common for all hydrocarbons, and volatile organic compounds (VOCs).

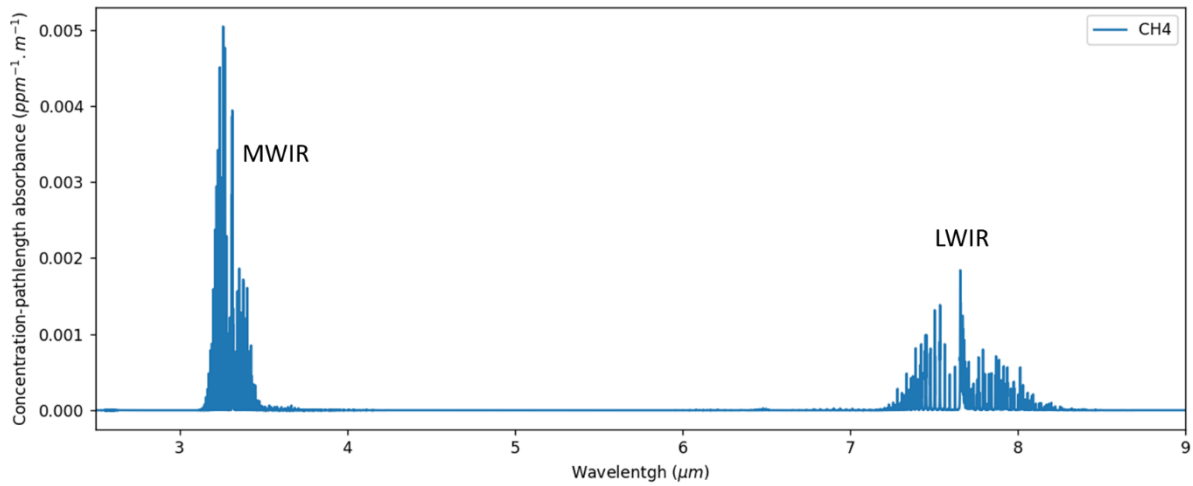

Figure 1: Concentration-pathlength absorbance of CH_4 (derived from the HITRAN database [2], T=296K, p=1atm)

In addition, LYNRED will soon launch another IR sensor for Continuous Emission Monitoring System (CEMS): This product, PICO640S BB 7-14 is an uncooled micro-bolometer array (VGA/17µm), targeting the methane absorption spectrum around 7.7µm.

2. HOW TO DETECT METHANE IN THE INFRARED SPECTRUM

An OGI camera is able to visualize a gas plume by thermal contrast with respect to the background. Let us model simply this phenomenon. An infrared camera with spectral response $S(\lambda)$ captures an image of a plume of gas X (e.g. methane), with absorbance $\alpha(\lambda)$ (in $ppm^{-1}.m^{-1}$), concentration c_X (in ppm), temperature T_G, and pathlength L (in m). In our model, we neglect the influence of air (an assumption valid for short viewing distances $d \leq 2m$).

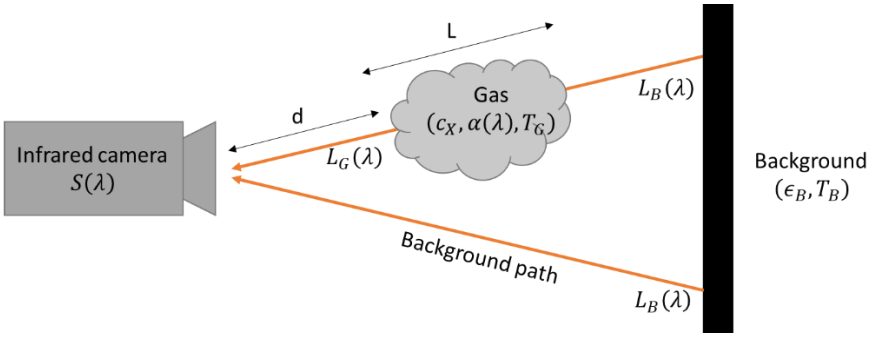

Figure 2: Schematic of the simplified OGI setup

We model the background as a uniform black body of emissivity $\epsilon_B \approx 1.0$ at the temperature T_B=T_{air}. Writing $L_0(\lambda, T)$ as the blackbody luminance (Planck's law, expressed in W/m2/sr/nm) at the temperature T, we express the background luminance $L_B(\lambda)$ in the equation below. Note that the reflected luminance from the environment, which takes into account the environment temperature and emissivity is neglected because $(1 - \epsilon_B) \ll 1$ and $T_{env} \approx T_B$.

$$L_B(\lambda, T_B) = \epsilon_B L_0(\lambda, T_B) + (1 - \epsilon_B)\epsilon_{env} L_0(\lambda, T_{env}) \approx L_0(\lambda, T_B)$$

We express $L_G(\lambda, c_X L)$ as the luminance along the optical path through the gas, which corresponds to the emission from the background, absorbed by the gas, as well as the emission from the gas itself. The absorbance of the gas (and also its emittance) along L is modeled by a Beer-Lambert law: $e^{-\alpha(\lambda)c_X L}$.

$$L_G(\lambda, c_X L) = e^{-\alpha(\lambda)c_X L}(\lambda) L_B(\lambda, T_B) + \left(1 - e^{-\alpha(\lambda)c_X L}\right) L_0(\lambda, T_G)$$

We plot in Figure 3 the luminance curve $L_G(\lambda, c_X L)$, for a plume of CH_4, with $c_X L$ = 1000 ppm.m, T_B = T_{ref} = 296 K ; and $\Delta T = T_G - T_B = +10$ K.

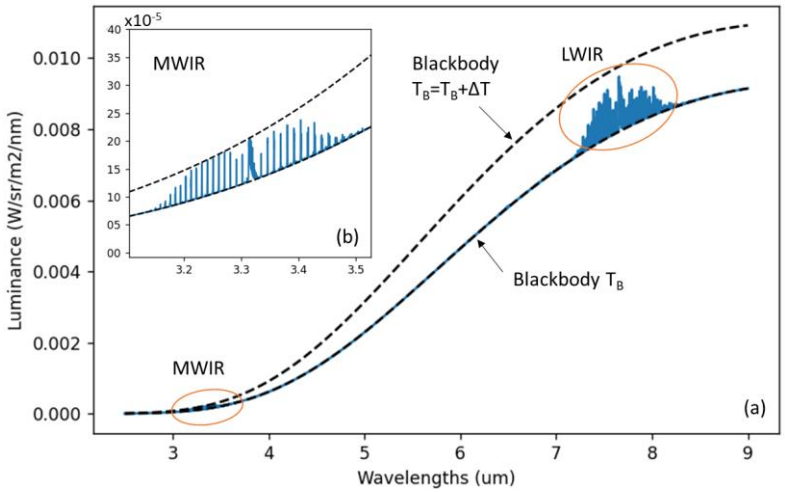

Figure 3: (a) Luminance L_G along the optical path through a CH_4 plume, with $c_X L$ = 1000 ppm.m, and ΔT =+10K. (b) Zoomed view on the MWIR absorption range

The luminance curve is bounded by the luminance of the background and the luminance of a black body at gas temperature (dashed curves). In other words, the more the gas temperature differs from the background temperature, the easier it will be to detect. On this temperature range, thermal contrast $\Delta L_0(\lambda, \Delta T) = L_0(\lambda, T_G) - L_B(\lambda, T_B)$ is weaker in MWIR band compared with the LWIR band (as seen in subfigure (b). However, the MWIR band benefits from strong absorbance of CH_4. Finally, by writing $\tau(\lambda, c_X L) = 1 - e^{-\alpha(\lambda)c_X L}$ as the transmission of the gas plume, we can write the luminance contrast between the gas and the background:

$$\Delta L(\lambda, c_X L\ ) = \tau(\lambda, c_X L)\big(L_0(\lambda, T_G) - L_B(\lambda)\big) = \tau(\lambda, c_X L)\Delta L_0(\lambda, \Delta T)$$

The EOLE sensor is a cooled hot-MWIR photonic sensor, with a 3.2-3.55µm band-pass cold filter. The quantum efficiency $QE(\lambda)$ of EOLE in the 3.2-3.55µm band is 70% in average (typical). Let us model EOLE's OGI performances under the BLIP model (Background Limited Infrared Photodiode). In such a model, the noise σ_{BLIP} is dominated by the shot-noise from the background, compared with other noise contributors (such as signal, √kTC and readout noise). This model is valid for cooled infrared detectors with proper exposure time t_{exp} and well fill.

$$\sigma_{BLIP}(T_B) = \sqrt{t_{exp} A_p T_{opt} \Omega \int \frac{\lambda}{hc} QE(\lambda) L_0(\lambda, T_B)\, d\lambda}$$

With $A_p = p^2$ the pixels' sensitive surface area, $p = 15\mu m$ the pixel's pitch, T_{opt}=90% the objective lens average transmission assumed flat on the interest waveband, Ω the solid angle of the objective lens, defined from its f/# (f-number) of the cold stop: $\Omega = 2\pi(1 - \cos(\text{asin}(1/2f\#)))$. The Contrast-to-Noise Ratio (CNR) at a given ΔT is calculated using the following expression:

$$CNR_{\Delta T}(c_X L) = t_{exp} A_p T_{opt} \Omega \frac{\int \frac{\lambda}{hc} QE(\lambda) \tau(\lambda, c_X L)\big(L_0(\lambda, T_B + \Delta T) - L_B(\lambda)\big)\, d\lambda}{\sigma_{BLIP}(T_B)}$$

The Noise Equivalent Concentration Length (NECL, expressed in ppm.m) is a metric that quantifies a camera sensitivity to a gas' concentration-pathlength, proposed by FLIR [3]. It depends mainly on the gas to background thermal contrast. FLIR defines NECL with a thermal contrast ΔT=10K at a 1m viewing distance. We define NECL as:

$$CNR_{10K}(NECL) = \pm 1$$

We plot in Figure 4, the $CNR_{\Delta T}(c_X L)$ curves for EOLE f/1.3 with 16ms exposure time. NECL is obtained when the ΔT=10K curve crosses the dotted line (CNR=1), which gives a native NECL of 24 ppm.m (typical). NECL is usually given with noise reduction post-processing (spatio-temporal). We use a typical denoising factor of x1.64: this gives us a post-processed NECL of 14.5 ppm.m.

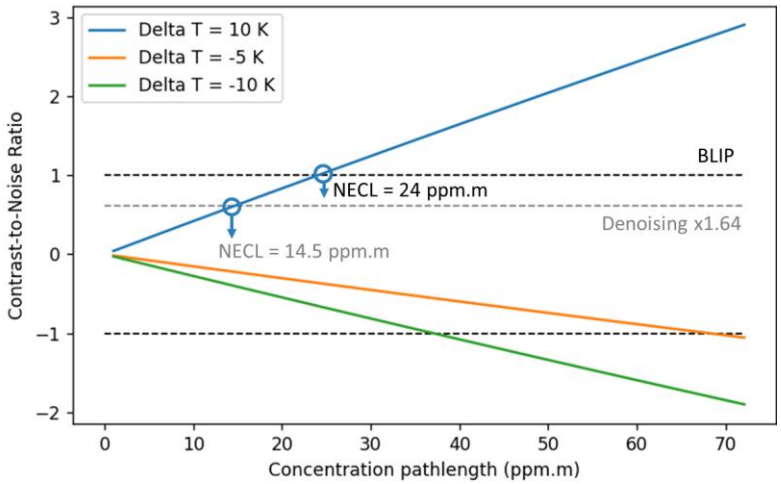

Figure 4: EOLE f/1.3 gas-to-background contrast-to-noise ratio, for different ΔT.

NECL is, by default, given at a gas-to-background temperature difference ΔT=+10K. The gas plume gets harder to detect when the gas temperature gets close to the background temperature. We plot in Figure 5, the EOLE's NECL value as a function of temperature difference.

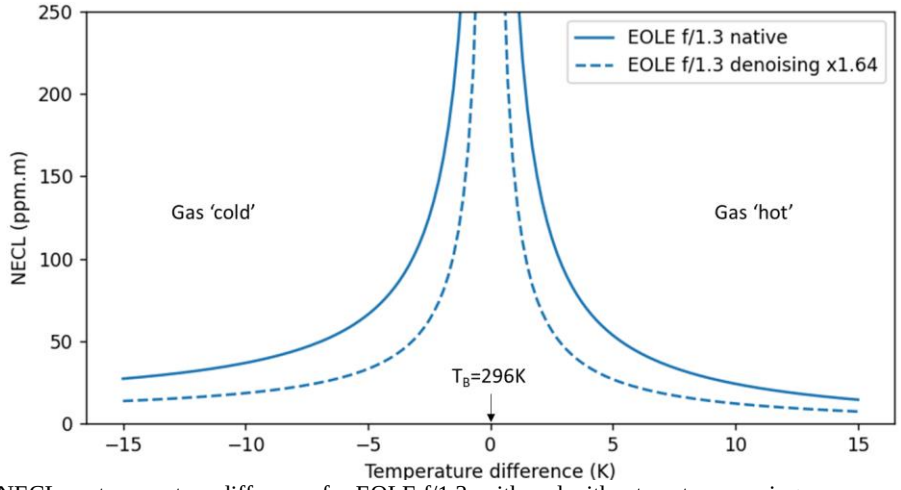

Figure 5: NECL vs. temperature difference for EOLE f/1.3, with and without post-processing

US and EU rules requires OGI cameras to have a Minimal Detectable Leak Rate (MDLR), given in g/h (<17g/h LDAR Type 1). It means that the OGI camera must render an image in which a camera operator can detect a gas leak. MDLR is metric that can be highly biased by both the operator's visual acuity and the 'controlled' laboratory conditions such as windspeed intensity and orientation, exit velocity and outlet diameter, etc., which aren't properly defined in the regulation. A leak plume can be detected if an operator can resolve the plume with sufficient CNR. To assess this, one need to model such a plume in order to generate a three-dimensional concentration map that properly models the dispersion of the pollutant. This concentration map can be projected into a concentration path-length (CL) sampling array, representative of a noise-free camera image, which has to be compared with the camera's NECL at the given ΔT.

We use the simple Gaussian dispersion plume model, as described by M. R. Beychok [4]. Such a model accurately describes experimental data (averaged OGI images) from controlled leaks, as shown in reference [5]. However, it generation smooth and continuous plumes, and thus cannot generate video sequences that carries the displacement of inhomogeneous 'patches' of higher and lower concentrations. Let us consider an outlet at the height h_0, which emits the pollutant (e.g. methane) at a rate Q (in g/s), and a horizontal wind in the x direction, at a wind-speed u (in m/s) as drawn in Figure 6.

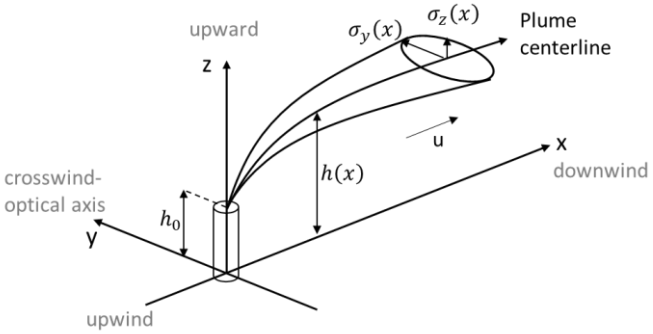

Figure 6: Geometry of the Gaussian plume model

The concentration profile of the pollutant along the plume centerline is assumed to have a Gaussian dispersion. The coordinate systems is defined along the wind direction: with x, y, z being the downwind, crosswind, and vertical directions, respectively. The concentration map $C(x, y, z)$ in g/m^3 is expressed as the following.

$$C(x,y,z) = \frac{Q}{u} \cdot \frac{f(x,y)}{\sigma_y(x)\sqrt{2\pi}} \cdot \frac{g(x,z)}{\sigma_z(x)\sqrt{2\pi}}$$

The crosswind $f(x,y)$ and vertical $g(x,z)$ dispersions are Gaussian models that are expressed in reference [4], with parameters that depends on the atmospheric stability class proposed by F. Pasquill. We consider typical laboratory conditions: wind-speed <2m/, daytime with slight solar radiation (<350W/m^2), which corresponds to Pasquill's stability class B: '*moderately unstable'*. The plume rise $\Delta h(x) = h(x) - h_0$ is not a critical parameter in our OGI sensitivity model, so we will consider a very simple expression, valid for non-buoyant jet plumes, among the variety of those proposed by Briggs [6]. The momentum flux parameter $F_m \approx v_g^2 r_0^2$ is given with the gas' exit velocity v_g (typ. 5m/s) and the outlet radius r_0 (typ. 1/8'').

$$\Delta h(x) = 2.3\, F_m^{1/3} u^{-2/3} x^{1/3}$$

We now consider an OGI camera that records an image of the plume with an optical axis parallel to the y-crosswind direction. To simplify the problem, we ignore perspective effects so that we can simply integrate the optical pathlengh in the y-direction. The expression of the concentration-pathlength $CL(x,z)$ in objet space (given in g/m^2) can be simplified as such:

$$CL(x,z) = \int C(x,y,z)dy = \frac{Q}{u} \cdot \frac{g(x,z)}{\sigma_z(x)\sqrt{2\pi}}$$

Conversion from object space (x, z in m) to image space (i, j in pixels) is done using the optical magnification M (in pix/m), assuming no optical distortions.

$$M = \frac{FL}{p.d}$$

Where FL is the lens' focal length (in mm), p is the pixel's pitch (in mm/pix) and d is the camera-plume viewing distance (in m). In Figure 7(a), we show an example of a plume image simulation from a Q=17g/h methane leak, h_0=0.2m, with a horizontal wind u=0.7m/s; seen with a 640x512/15µm OGI camera with a FL=30mm lens, at a 2m viewing distance.

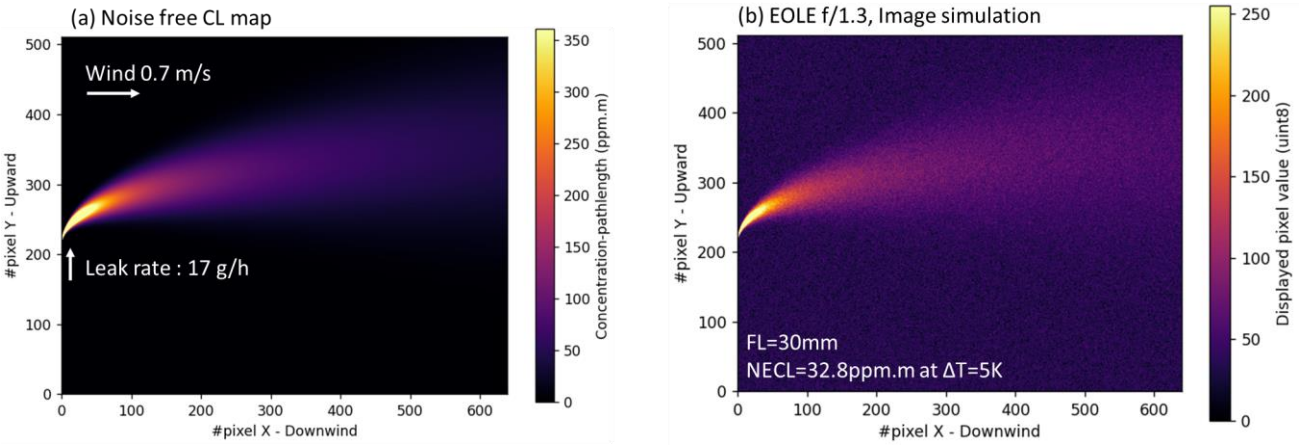

Figure 7: Leak image simulation (a) Noise free CL map, (b) EOLE f/1.3 with NECL=32.8ppm.m

Such a CL image is to be compared with the camera's NECL at the proper ΔT. We show in Figure 7(b), an image rendering of the same plume of methane using an EOLE f/1.3 camera. NECL values are taken at ΔT=5K, with the x1.64 noise reduction enabled. EOLE shows a clear image of the 17g/h methane leak: any operator should properly resolve the plume. It suggests that EOLE f/1.3 would be compliant with both EU's LDAR type 1 (>17g/h, ΔT unspecified) and US regulations (>19g/h, ΔT=5K).

The Minimal Detectable Leak Rate (MDLR) criterion is unclear, and based on the camera operator acuity. We propose to define N_{pix} as the number of pixels where $CL(i,j) > NECL$. Reference [5] suggests to set the criterion at N_{pix}=400pix, which corresponds to an equivalent square of width 20pix. Although, we argue that a 9x9 criterion is reasonable based on our experience, especially if the operator is assisted visually with proper image representation (see Section 4). We plot in Figure 8, the square-equivalent width $\sqrt{N_{pix}}$ of the detected plume for EOLE f/1.3. MDRL values are obtained when $\sqrt{N_{pix}}$ reaches a given threshold: 1.36 g/h for the 20x20 criterion; and 0.67 g/h for the 9x9 criterion.

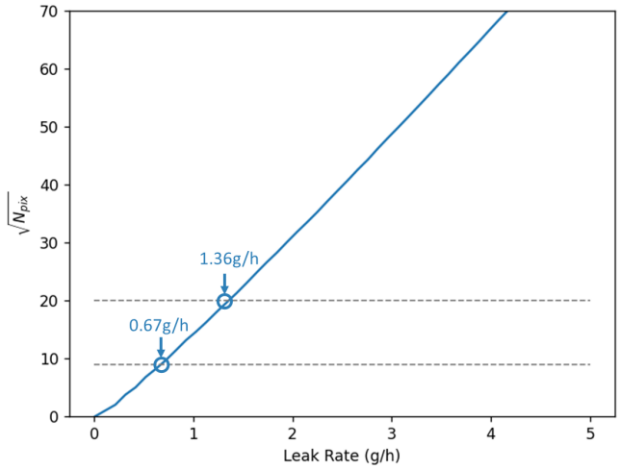

Figure 8: Square-equivalent width of the detected plume as a function of the leak rate

Absolute values of MDLR are highly biased due to the conditions, notably winds and viewing conditions. Indeed, wind speed and orientation dramatically changes the dilution of pollutant, and thus the projected CL; the distance and FL modifies the optical magnification, and thus the quality of the CL sampling at the vicinity of the plume exit. Moreover, the smooth and continuous Gaussian plumes cannot generate patches of higher pollutant concentration, which would increase the pixel count in a real turbulent plume. It means that our MDLR estimations are overestimated.

3. LABORATORY LEAK RATE EVALUATION

As explained earlier, laboratory tests are performed with a controlled leak of known rate, where the gas in seen by contrast to a uniform background. Figure 9 is a photograph of the laboratory test setup at SENSIA's facilities (Madrid, Spain).

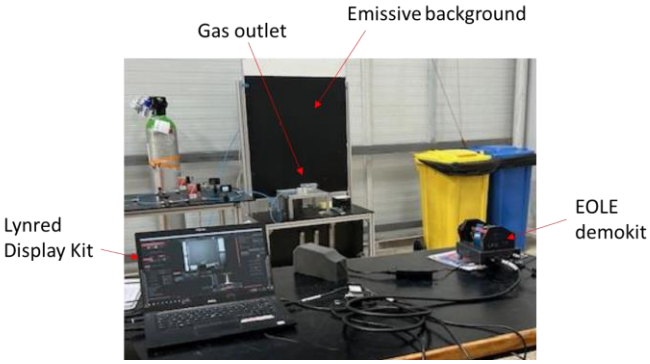

Figure 9: Laboratory test setup

We use EOLE f/1.3 with a suboptimal FL 25mm f/2 lens. Note that better performances are expected with a f/1.3 lens, properly adapted to the sensor's cold stop aperture. The image is simply processed with a non-uniformity correction (NUC), and displayed linear tone-mapping as a grayscale image, through LYNRED's Display Kit user interface. This is the native EOLE configuration, without noise reduction post-processing. Figure 10 shows snapshots of EOLE's video stream with decreasing leak rates of 0.5 L/min, 0.2 L/min and 0.04 L/min of pure methane, which is converted to 19.8 g/h, 7.9 g/h and 1.6 g/h respectively (assuming 1 bar air pressure, and 296 K air temperature). Note that, in this case, the gas appears darker than the background: it means that the gas is colder than the background ($\Delta T<0$). Real gas plumes have patches, unlike our smooth Gaussian model.

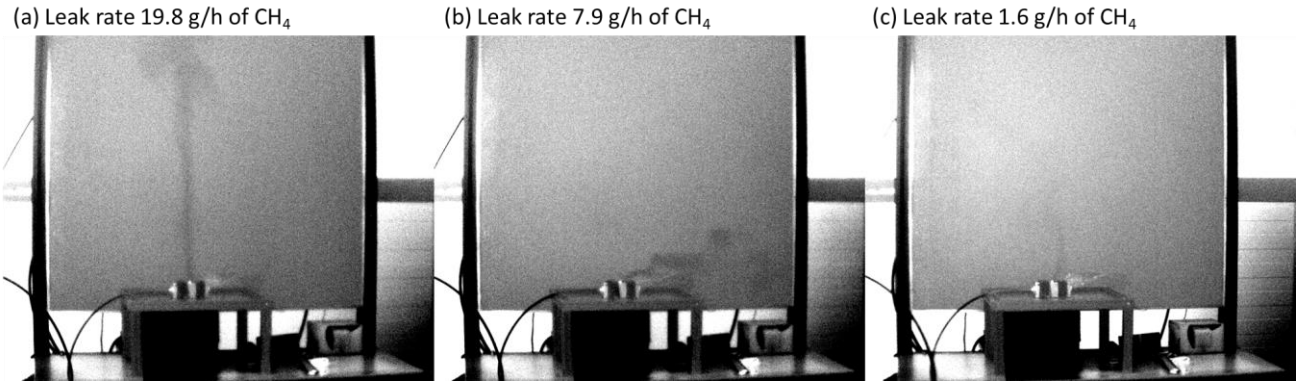

Figure 10: Controlled leaks of methane viewed with EOLE using a 25mm f/2 lens with a uniform background. Leak rates (a) 19.8 g/h, (b) 7.9 g/h and (c) 1.6 g/h.

In accordance with the theoretical study, the gas-to-background contrast decreases with the leak-rate, which makes the gas leak harder to detect (CL closer to the camera's NECL). While the 1.6 g/h leak is easily perceptible through the computer video display with this simple processing, detecting fainter leaks will require new key image processing steps, such as efficient spatio-temporal denoising, and perception-enhanced image rendering, such as colorization. Moreover, complex background such as those found in real situations will make the leak detection harder, notably because of the broader display dynamic of the background.

4. ATI EOLE VIDEO PIPELINE

In addition to the EOLE sensor, delivering high-quality raw image, LYNRED is set to launch the ATI EOLE in April 2025, a next-generation Advanced Thermal Imager (ATI) module specifically designed to address the requirements of modern methane detection frameworks. The ATI EOLE integrates embedded image processing algorithms that perform real-time corrections on raw thermal data, delivering high-quality, corrected thermal images. This advanced image processing capability enhances the accuracy and reliability of methane detection in compliance with regulatory standards.

Furthermore, the ATI EOLE is engineered to facilitate seamless system integration, providing camera manufacturers with a streamlined solution that accelerates product development cycles. By reducing the need for extensive post-processing and external calibration, the ATI EOLE enables system integrators to shorten their Time-to-Market (TTM) while ensuring that their detection platforms meet the latest regulatory mandates. This new product offer also reduces the Total Cost of Ownership (TCO) thanks to the lack of necessity to develop an image correction board.

This technological advancement represents a critical step in bridging the gap between regulatory requirements and industrial implementation, offering a field-proven solution that enhances methane detection accuracy, operational efficiency, and regulatory compliance in the oil and gas sector.

Embedded ATI EOLE video processing pipeline, schematized in Figure 11, consist of NUC, bad pixel replacement (BPR), spatial and temporal denoising, digital details enhancement (DDE), tone mapping, 7 pre-defined color-maps (Lifeinred™ color palettes) and up to 8 user color-maps for image colorization.

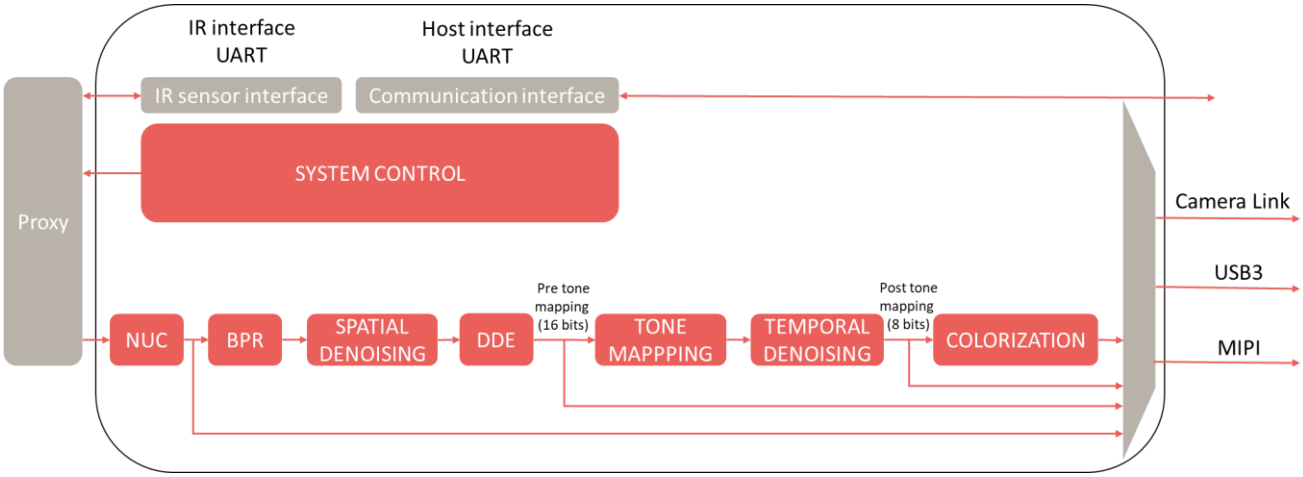

Figure 11 : Main functional blocks of the image signal processor (ISP). This ISP embedded in ATI EOLE is specifically designed to ensure optimized image quality and best compromise between scene dynamic and NECL.

NUC, BPR and destripping are mandatory to achieve a good image quality. On the other hand, temporal and spatial denoising, implemented on ATI EOLE, allows to improve CNR by a typical factor of x1.64, in order to detect faint gas leaks (see Figure 4). This embedded video pipeline correction is a great starting point for further gas analysis and gas leak quantification.

The pipeline features image rendering steps: tone-mapping and colorization, designed to enhances the perception of the gas plume on the image displayed to the camera operator. An example is shown in Figure 12, with a methane leak of 931g/h (super emitter), recorded at the NaTran facilities (Paris, France) with the suboptimal FL 25mm f/2 lens.

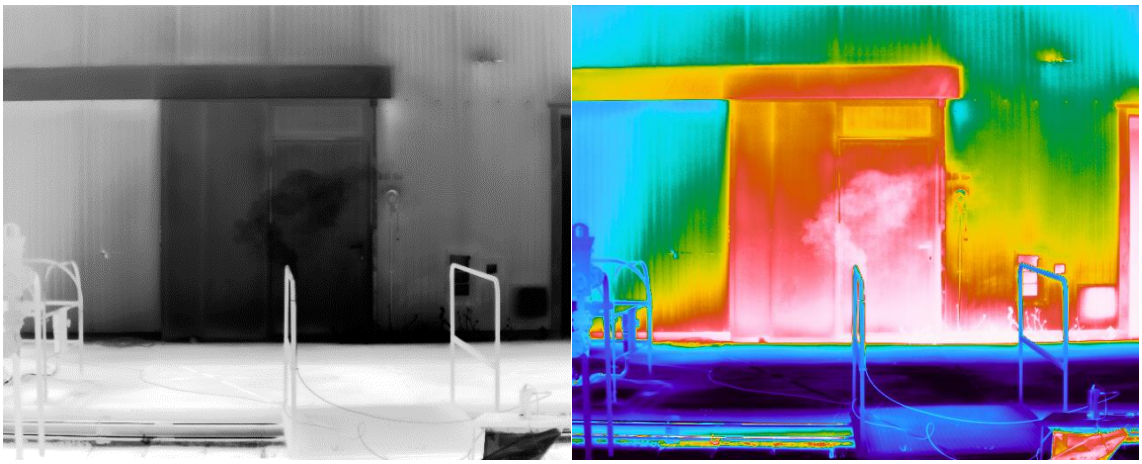

Figure 12 : Embedded ATI EOLE algorithms with corrected tone-mapped image for a leak of 931g/h (assuming 1 bar and T=296K) at a distance of 9.5m; (left) with black-hot and (right) Lifeinred™ Inspect inverse color palettes.

These image enhancements is crucial to help visualizing the gas leak in difficult environmental conditions such as small gas plume. In even more difficult conditions (complex background, strong wind, small ΔT, etc.), additional image processing may be needed to visualize the gas.

5. VISUAL ENHANCEMENTS THANKS TO LYNRED TOOLBOX ALGORITHMS

The Lynred Toolbox software [7] features additional image post-processing algorithms and visualization modes dedicated for OGI, including high sensitivity modes and background removal (with or without edges enhancement). Those advanced algorithms help to probe that EOLE is sensitive enough to detect gas leaks below Type 1 LDAR, as shown in Figure 13,

which are difficult conditions for which the gas is not easily perceptible on corrected images alone. Lynred Toolbox algorithms could also be used as a starting point for end-users interested in background removal for gas quantification.

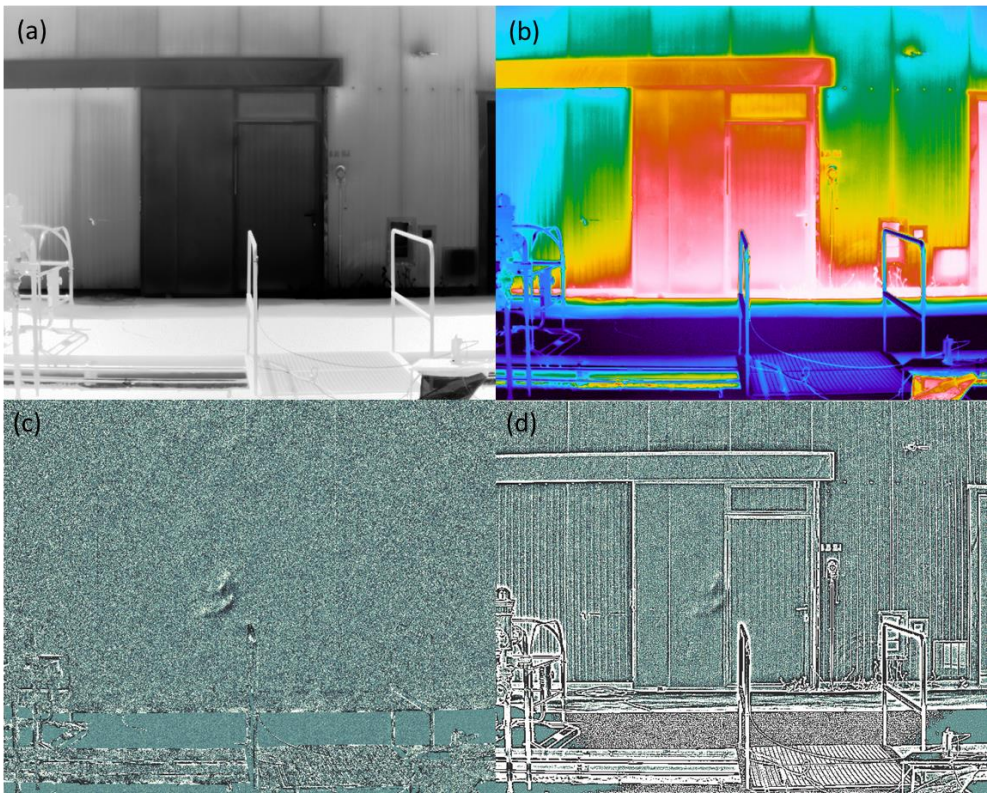

Figure 13 : Lynred Toolbox gas visualization algorithms for a gas leak of 15.9g/h (assuming 1 bar and T=296K) at a distance of 9.5m. (a, b) ATI embedded modes. (c) high sensitivity mode with background removal and with Lifeinred™ serenity color palette. (d) high sensitivity mode with edges enhancement to visualize both the gas and the surrounding.

6. ANSWERING TO THE SWAP NEEDS VIA PLUGUP™

Beyond its integration of high-quality embedded image processing algorithms, ATI EOLE has been specifically engineered to meet Size, Weight, and Power (SWaP) constraints, a critical requirement for modern airborne and unmanned aerial vehicle (UAV) applications. The system features an ultra-low power consumption of less than 4.4 Wdc, addressing the increasing demand for energy-efficient solutions in mobile and autonomous platforms. Additionally, the ATI EOLE has a total weight of only 388 grams, ensuring compatibility with weight-sensitive applications while maintaining high-performance imaging capabilities.

Moreover, the ATI EOLE thermal imaging system is built upon LYNRED's newly developed PlugUp™ platform, a modular and scalable foundation designed to streamline the integration process for system developers. The PlugUp™ platform offers a compact and lightweight design, coupled with three standardized mechanical interfaces, enabling system integrators to accelerate development cycles and minimize time-to-market (TTM).

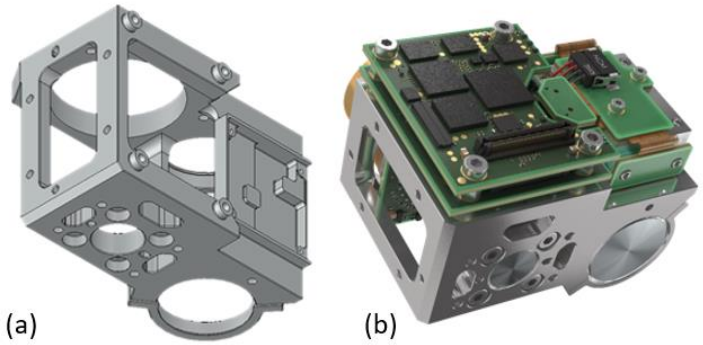

Figure 13: (a) Empty PlugUp™ platform that hosts various LYNRED sensors and ATI. (b) ATI EOLE with integrated processing board

The PlugUp™ platform ("Plug & Upgrade") represents LYNRED's new standard across its infrared sensor portfolio, ensuring long-term compatibility and ease of system evolution. By maintaining a consistent form factor across successive product generations, the platform enables developers to design systems based on one sensor model and seamlessly transition to next-generation technologies without requiring significant hardware modifications. This backward and forward compatibility enhances flexibility, reduces redesign costs, and future-proofs thermal imaging applications for evolving industry requirements. The PlugUp™ platform also hosts the new SXGA (1280x1024), 7.5µm pixel pitch, MWIR product named SEEGNUS SL [8].

7. CONCLUSION

In this paper, we introduced EOLE: a state-of-art HOT-MWIR VGA imaging core dedicated for hydrocarbon OGI. An easy to use module, called ATI EOLE, includes an advanced video processing pipeline, which provides to the user corrected images enabling the detection and quantification of a gas leak. ATI EOLE is a SWaP solution, integrated into LYNRED's PlugUp™ platform, which ensures backward and forward compatibly, for faster system integration.

We demonstrated how ATI EOLE is able to image a methane (CH_4) plume, with enhance sensitivity, in order to detect and locate faint gas leak. Our technology is compliant with the European EU/2024/1787 and the US EPA QuadOs regulation, as proven by a theoretical study on key performance metrics of OGI cameras, laboratory performance evaluation, as well as field demonstration on controlled leaks.

While our study was limited to a given set of conditions, and a suboptimal f/2 objective lens compared to EOLE's f/1.3 cold stop aperture, we were able to test our solution in hard conditions for detection such as small leaks, complex backgrounds etc. For such conditions, we provide additional software visualization algorithms in LYNRED Toolbox, to enhance the perception of the leak. In the future, we will compare EOLE and Lynred's upcoming uncooled LWIR solution, based on simulation and field experiments. Further investigations could also explore the required algorithms in order to comply with the regulation at a long distance, which may enhance our understanding of the OGI capabilities in airborne solutions.

ACKNOWLEDGEMENTS

The authors acknowledge that the images used in this study were captured within the facilities of NaTran (Paris, France) and Sensia (Madrid, Spain). We appreciate the support provided by NaTran: Néméhie Lawson and Salim Lachichi in granting access to their premises for this research. We are thankful for Juan José Frutos Andreu and the Sensia team for their insight and support.

ABBREVIATIONS

The main abbreviations used in this paper are listed below:

ATI	Advanced Thermal Imager
BLIP	Background Limited Infrared Photodetector
BPR	Bad Pixel Replacement
CEMS	Continuous Emission Monitoring System
CH_4	Methane
CL	Concentration Length, given in ppm.m
CNR	Contrast-to-Noise Ratio
DDE	Digital Details Enhancement
EPA	Environmental Protection Agency
FL	Focal Length, given in mm
ISP	Image Signal Processor
LDAR	Leak Detection And Repair
LWIR	Long Wave InfraRed
MDLR	Minimal Detectable Leak-Rate, given in g/h or L/min
MWIR	Middle Wave InfraRed
NECL	Noise Equivalent Concentration Length, given in ppm.m
NUC	Non Uniformity Correction
OGI	Optical Gas Imaging
QE	Quantum Efficiency
SWaP	Size Weight and Power
TCO	Total Cost of Ownership
TTM	Time-to-Market
UAV	Unmanned Aerial Vehicle
VGA	Video Graphics Array (640x512)

REFERENCES

[1] Environmental Protection Agency, OOOOa,b,c ; Appendix K : Determination of Volatile Organic Compound and Greenhouse Gas Leaks Using Optical Gas Imaging (Final Rule 2022). [Online]. Available: https://www.ecfr.gov/current/title-40/chapter-I/subchapter-C/part-60/appendix-Appendix%20K%20to%20Part%2060

[2] L. S. Rothman et al., "The HITRAN 2004 molecular spectroscopic database," J. Quant. Spectrosc. Radiat. Transf., vol. 96, no. 2, Dec. 2005, doi: https://doi.org/10.1016/j.jqsrt.2004.10.008.

[3] J. Sandsten, U. Wallgren, S. Barenthin, and Hagman Henning, "Optical gas imaging standards for sensitivity and detection of gases," presented at the A&WMA's 108th Annual Conference, Raleigh (North Carolina), Jun. 2015.

[4] M. R. Beychok, Fundamentals of Stack Gas Dispersion, 4th edition.

[5] A. P. Ravikumar, J. Wang, and A. R. Brandt, "Are Optical Gas Imaging Technologies Effective For Methane Leak Detection?," Environ. Sci. Technol., Nov. 2016, doi: https://doi.org/10.1021/acs.est.6b03906.

[6] G. A. Briggs, "CONCAWE meeting: discussion of the comparative consequences of different plume rise formulas," Atmos. Envir., 1968.

[7] B. Louvat, H. Delestre, M. Pouchol, C. Combet, and J. Walther, "Advanced Software Solutions for IR images," presented at the SPIE Defense + Commercial Sensing, Orlando, Florida, United States: SPIE, Apr. 2025.

[8] Y. Reibel, N. Péré-Laperne, A. Brunner, A. Saintoyant, A. Collier, and J. Coussement, "LYNRED's SWAP product lines using the High Operating Temperature technology," presented at the SPIE Defense + Commercial Sensing, Orlando, Florida, United States: SPIE, Apr. 2025.